Supplemental Document

Optics Letters

# Easily scalable multi-color DMD-based structured illumination microscopy: supplement

**Daozheng Gong,[1,2] Chufan Cai,[3] Eli Strahilevitz,[4] Jing Chen,[5] and Norbert F. Scherer[2,6,7,*]**

[1] *Graduate Program in Biophysical Science, University of Chicago, Chicago, Illinois, 60637, USA*
[2] *Institute for Biophysical Dynamics, University of Chicago, Illinois, 60637, USA*
[3] *Graduate Program in Cancer Biology, University of Chicago, Chicago, Illinois, 60637, USA*
[4] *University of Chicago Laboratory Schools, Chicago, Illinois, 60637, USA*
[5] *Department of Medicine, The University of Chicago, Chicago, Illinois 60637, USA*
[6] *Department of Chemistry, University of Chicago, Chicago, Illinois, 60637, USA*
[7] *James Franck Institute, Chicago, Illinois, 60637, USA*
[*] *nfschere@uchicago.edu*



Supplement DOI: https://doi.org/10.6084/m9.figshare.24721821

Parent Article DOI: https://doi.org/10.1364/OL.507599

# Easily scalable multicolor DMD based structured illumination microscopy: supplemental document

## 1. DIFFRACTION CHARACTERISTICS OF DMD

The periodic discrete element structure of the micro-mirror array makes the DMD behave as a diffraction grating. As Fig. 1A shows, the micro-mirror array can be considered as a 2-dimensional blazed grating, with a line spacing of $\delta = 7.56\ \mu$m in both directions. Each micro-mirror is tilted by an angle of $\gamma = 12^\circ$ along its diagonal. In practice, we rotated the whole DMD by $45^\circ$ about its surface normal (i.e., z axis) so that the tilting is along the y axis (i.e., vertical axis).

Fig. S1 shows a detailed ray tracing schematic of the incident and diffracted rays of the DMD. In this coordinate system, the lattice vector $\vec{d}$ joining two adjacent micro-mirrors is:

$$\vec{d} = (\frac{\sqrt{2}}{2}\delta, \frac{\sqrt{2}}{2}\delta, 0). \tag{S1}$$

The incident ray $\vec{\alpha}$ and diffracted ray $\vec{\beta}$ are defined as

$$\vec{\alpha} = -(\sin\theta_0\cos\phi_0, \sin\theta_0\sin\phi_0, \cos\theta_0),\ \vec{\beta} = (\sin\theta_1\cos\phi_1, \sin\theta_1\sin\phi_1, \cos\theta_1), \tag{S2}$$

where $(\theta_0, \phi_0)$ are the angles of $\vec{\alpha}$ between the $z$ and $x$ axis, and $(\theta_1, \phi_1)$ are the angles of $\vec{\beta}$ between the $z$ and $x$ axes. The optical path difference between two adjacent micro-mirror pixels are given by:

$$\Delta = \vec{d}\cdot\vec{\alpha} + \vec{d}\cdot\vec{\beta} = \frac{\sqrt{2}}{2}\delta(\sin\theta_1(\cos\phi_1 + \sin\phi_1) - \sin\theta_0(\cos\phi_0 + \sin\phi_0)), \tag{S3}$$

and the diffraction pattern is given by the grating equation:

$$\Delta = m\lambda_{ex}, m \in \mathbb{Z}, \tag{S4}$$

where $m$ is the diffraction order. At the blaze condition, one of the diffraction orders should overlap with the direct reflection of a single micro-mirror, that is:

$$\theta_0 - 2\gamma = \theta_1,\ \phi_0 = -\phi_1, \tag{S5}$$

and this will lead to maximum optical power concentrated to the single diffraction order.

In practice, in order to maintain the the parallelism between the optical path and optical table, we constrain the incident light to be in a plane perpendicular to the y axis, i.e. $\phi_0 = 0$. In addition, to make the blaze diffraction parallel to the optical axis, a blaze condition at $\theta_1 = 0^\circ$ will be ideal. This leads to $\theta_0 = 2\gamma = 24^\circ$. Inserting these two constraints into the diffraction equation S4 gives the wavelengths of excitation light that satisfy the blazing condition:

$$\lambda_{ex} = -\frac{\sqrt{2}\delta\sin 2\gamma}{2m}, m \in \mathbb{Z}. \tag{S6}$$

Apparently, the blaze condition can only be fulfilled with certain discrete wavelengths. In Table S1, we list some of those wavelengths that give rise to the blaze diffraction directed perpendicular to the DMD surface. Note that common laser wavelengths do not exactly match, which means the setup will then deviate from the ideal blazing case. In our system, we set the incident angle of the 532 nm beam on DMD to be $\theta_0 = \theta_{0G} = 23.46^\circ$ and use the $m = -4$ order diffraction at $\theta_1 = \theta_{1G} = 0^\circ$ as the illumination beam that goes into the microscope.

An additional blazed grating is used to compensate the deviation of the other wavelengths beams that we use in this study, which cover most of the range of visible light. As shown in Figure S2, by adjusting the incident angle $\psi_0$ of the laser beam onto the blazed grating, the deviation $\Delta\theta_1$ of all the other wavelength beams are very close to zero and thus propogating collinearly with the 532 nm beam.

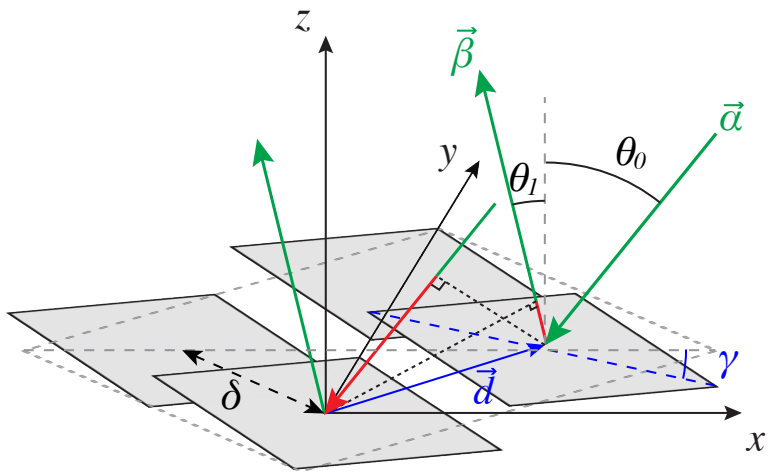


**Fig. S1.** Schematic of light propagating onto and from a DMD including angles of incidence and diffraction. See text for details of the symbols. The z axis is perpendicular to the plane of the DMD and x and y axes are in the plane of the DMD. This coordinate system is the same as in Fig 1A. The red line segments represent the optical path difference of incident rays $(\vec{d} \cdot \vec{\alpha})$ or diffracted rays $(\vec{d} \cdot \vec{\beta})$ for two adjacent micro-mirrors.

| Blaze order | Wavelength (nm) |
|---|---|
| -2 | 1087.2 |
| -3 | 724.8 |
| -4 | 543.5 |
| -5 | 434.9 |
| -6 | 362.4 |

**Table S1.** Blaze orders and the corresponding blaze wavelengths that satisfy equation S6.

## 2. CHOICE OF THE BLAZED GRATING

To determine the ideal parameter (i.e., period, $d$, and blaze angle, $\nu$) of the blazed grating, we can first calculate the dispersion of a grating as $\frac{m_1}{d\cos(\psi_1)}$ [1], where $\psi_1$ is the diffraction angle of the grating, $m_1$ is the diffraction order, and $d$ is the grating period. The first order is desired to achieve the maximum efficiency. For a DMD with pixel size $\delta$, the dispersion along its diagonal direction can be similarly expressed as $\frac{2m}{\sqrt{2}\delta\cos(\theta_1)}$, where $\theta_1$ and $m$ are the diffraction angle and order of the DMD, respectively. In our case, $\theta_1$ is equal to $0^\circ$ and $m$ is equal to -4 as mentioned in supplementary Section 1. In a small wavelength range, the dispersion of the blazed grating and the DMD need to have opposite values to achieve dispersion compensation:

$$\frac{1}{d\cos(\psi_1)} + \frac{2m}{\sqrt{2}\delta} = 0. \tag{S7}$$

This equation only works in a small range of wavelengths and cannot be used to exactly determine the grating parameter for our multi-color imaging application. However, it indicates that a grating with relatively small line density (i.e. large $d$), such as 300 or 600 lines/mm, has to be chosen to not over compensate the dispersion caused by the DMD. In our work we chose the line density to be 600 lines/mm since the choices of commercially available 300 lines/mm gratings are limited.

After the $d$ is determined, the incident angle $\psi_0$ to achieve precise angle corrections for all 4 wavelengths used in our study can then be determined by numerical calculation from equations 3 and 4. As shown in Figure S2, $\psi_0 = 21.41^\circ$ when the line density is chosen to be 600 lines/mm. The diffraction angle $\psi_1$ can then be calculated to be $\psi_1 = 43.18^\circ$ from equation 3. To satisfy the blazed condition an ideal blaze angle $\nu$ for the blazed grating can be calculated as

$$\nu = \frac{\psi_0 - \psi_1}{2} = -10.88^\circ. \tag{S8}$$

The negative sign is an indication of the orientation of the blazed grating (as illustrated in Figure 2). In our work, we chose a blazed grating with 600 lines/mm grooves and a blaze angle of $8.62^\circ$ (Thorlabs GR13-0605) to most closely match the ideal parameters. Although it does not perfectly satisfy the blaze condition resulting in to energy loss, this mismatch does not affect the dispersion compensation function for our application. Since SIM has a modest requirement for illumination intensity, our setup can still achieve high quality live cell SIM imaging.

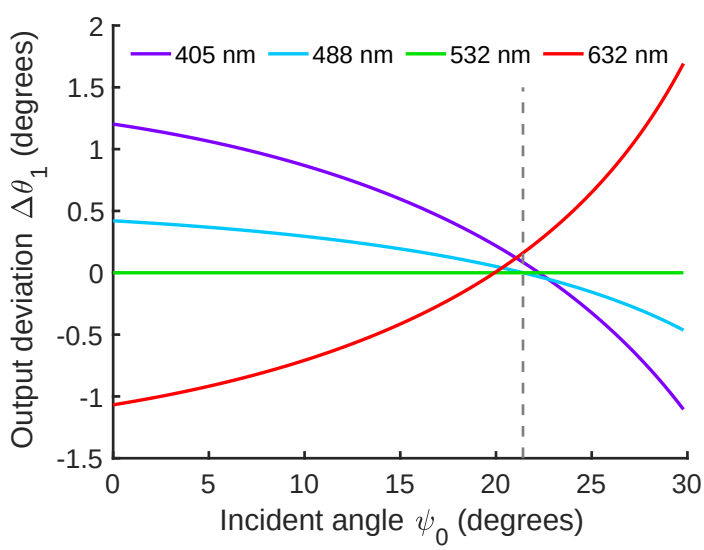


**Fig. S2.** Calculated output deviation $\Delta\theta_1$ of different wavelength beams versus the incident angle $\psi_0$ onto the blazed grating. The calculation is based on the equations 3 and 4.

## 3. ENERGY EFFICIENCY

In the gDMD-SIM method, a suitable choice of the blazed grating and the input angle can successfully counteract the angular dispersion effect of the DMD and allow aligning all the 4 color beams to the center of the optical path after the DMD. However, this alignment does not fully meet the blaze condition of the blazed grating and the DMD, which leads to relatively low energy efficiency. As a reference, we measured the beam power we used for live cell imaging at several critical locations along the beam path, as shown in Table S2.

| | L1 - L2 | L3 - L4 | L5 - L6 | sample plane |
|---|---|---|---|---|
| 642 nm | 72 mW | 25 mW | 1.8 mW | 1.2 mW |
| 532 nm | 20 mW | 11 mW | 3.0 mW | 2.0 mW |
| 488 nm | 76 mW | 48 mW | 2.5 mW | 1.6 mW |
| 402 nm | 62 mW | 24 mW | 0.6 mW | 0.4 mW |

**Table S2.** Illumination power of the laser beams at different locations. L1 - L2/L3 - L4/L5 - L6/ means the power was measured at the location between the lenses L1/L3/L5 and L2/L4/L6.

The 532 nm beam has the highest energy efficiency since it is closely aligned to the blazed condition of the DMD. The other 3 beams show significant energy loss, especially after the DMD, due to the deviation from their blaze condition. Despite this energy loss, in a 200$\mu$m diameter field of view, the illumination intensity still has a value of at leat 4 W/cm$^2$, which falls well into the common range for SIM excitation intensity [2].

The deviation from blaze condition could also lead to uneven intensities of the $\pm 1$ order beams for the SIM patterns, especially along the direction perpendicular to the y axis of the DMD. However, as we show in Figure S3, the max difference between the $\pm 1$ order beams is $\sim$ 24%. Although this can lead to a decrease of the modulation amplitude of the SIM pattern, in our experiment we do not oberserve noticeable problem from this intensity asymmetry.

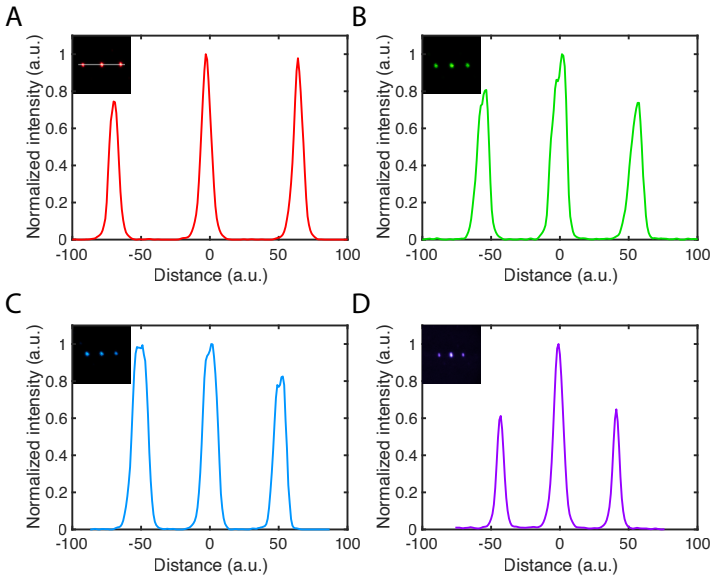


**Fig. S3.** Normalized intensities of the $\pm 1$ and 0 order beams for the 4 different wavelengths used in our study. The SIM pattern angle is chosen to be nearly paralleled to the y axis, in which case the diffracted beams show the strongest asymmetry. The intensities are measured along the gray line shown in the inset of A. The intensity ratio of the -1, 0 and +1 order beams are: (A) 642 nm channel: 0.74, 1, 0.98; (B) 532 nm channel: 0.8, 1, 0.74; (C) 488nm channel: 1, 1, 0.82; (D) 405nm channel: 0.61, 1, 0.65.

## 4. HARDWARE INFORMATION

| Component | Part number | Description |
|---|---|---|
| 642 nm laser | Spectra-Physics, Excelsior One 642 | 100 mW maximum power |
| 532 nm laser | Spectra-Physics, Millennia V | 5 W maximum power |
| 488 nm laser | Spectra-Physics, Excelsior One 488 | 100 mW maximum power |
| 405 nm laser | Spectra-Physics, Excelsior One 405 | 100 mW maximum power |
| DM1 | Semrock, Di03-R405-t1-25x36 | 414 nm long pass |
| DM2 | Semrock, Di03-R488-t1-25x36 | 500 nm long pass |
| DM3 | Thorlabs, DMSP550R | 550 nm short pass |
| L1 | Thorlabs, ACT508-100-A-ML | $f = 100$ mm |
| L2 | Thorlabs, ACT508-400-A-ML | $f = 400$ mm |
| Grating | Thorlabs, GR13-0605 | 600/mm, 500 nm blaze |
| L3 | Thorlabs, ACT508-200-A-ML | $f = 200$ mm |
| L4 | Thorlabs, ACT508-200-A-ML | $f = 200$ mm |
| DMD | Texas instrument, DLP9000X VIS WQXGA | $1600 \times 2560$ pixels |
| L5 | Thorlabs, ACT508-180-A-ML | $f = 180$ mm |
| HWP | Thorlabs, AHWP10M-600 | achromatic half wave plate |
| HWP mount | Newport,AG-PR100 | rotation stage for the HWP |
| L6 | Thorlabs, ACT508-250-A-ML | $f = 250$ mm |
| L7 | Thorlabs, ACT508-300-A-ML | $f = 300$ mm |
| L8 | Nikon, Eclipse-Ti (internal part) | $f = 200$ mm |
| Obj | Nikon, SR Plan Apo, 60X, 1.27 WI | |
| DM4 | Semrock, Di01-R405/488/532/635-25x36 | multi-edge dichroic mirror |
| Emission filter 1 | Semrock, FF01-446/510/581/703-25 | multi-band bandpass filter |
| Emission filter 2 | Chroma, ET590/33m | 590/33 nm bandpass filter |
| Emission filter 3 | Semrock, FF01-525/39 | 525/39 nm bandpass filter |
| sCMOS | Photometrics, Kinetix | |

**Table S3.** Information of the hardware components of the microscope setup. Here the HWP mounted on the motorized rotation stage was used to adjust the polarization of the beams in order to maximize the contrast of SIM patterns. Emission filter 1 is used for all channel imaging, while the emission filter 2/3 is added when imaging 532/488 nm channel to prevent signal cross talk.

## 5. SAMPLE PREPARATION

### A. Bead sample preparation

TetraSpeck 0.1 $\mu$m microspheres (ThermoFisher, T7279) were used to make the bead samples. Before using, the bead stock solution was first uniformly suspended by sonicating for 10 minutes. 4-6 $\mu$L of the bead suspension was applied on a pre-cleaned coverslip and air-dried overnight. 10$\mu$L of mounting medium was then applied to the fully dried coverslip. The coverslip was then placed on a precleaned microscope slide and sealed with nail polish. Note that although the tetraspeck microspheres display colors, our 405 nm wavelength laser does not match with any of the 4 excitation spectra of the beads. For these reasons we were only able to test 3 color imaging on the fluorescent beads.

### B. Cell sample preparation

Human BJ fibroblast cells were cultured in high-glucose DMEM (Life Technologies 10569) containing 10% fetal bovine serum (Life Technologies 26140) and penicillin-streptomycin in a 5% $CO_2$, 37°C, water humidified incubator. Before imaging, live cells were washed with PBS (Life Technologies 15140) and then trypsinized in 2.5 mL trypsin (0.05%, Life Technologies 25300) at 70-80% confluence before being moved to 35 mm glass bottom dishes (Mattek P35G-1.5-14-C) for microscopy imaging. Stainning solution was made by diluting Tubulin Tracker Deep Red (ThermoFisher Scientific, T34077) to 1×, CellMask Orange Actin Tracking Stain (ThermoFisher Scientific, A57247) to 2×, MitoTracker Green FM (ThermoFisher Scientific, M7514) to 100 nM, and Hoechst 34580 (ThermoFisher Scientific, H21486) to 5 $\mu$g/mL in growth media. For imaging, cells were incubated in 1 mL stainning solution for 30 minutes at 37°$C$, rinsed 5 times in FluoroBrite DMEM (ThermoFisher, A1896701), then imaged and analyzed in the FluoroBrite DMEM.

## 6. SIM RECONSTRUCTION AND SPATIAL RESOLUTION ENHANCEMENT

Three-beam interference configuration is adopted in the presented study. During a SIM image acquisition, a 6 pixel-period striped patterns with 3 different orientations (about the DMD normal) are displayed by the DMD. 6 phase shifted patterns are used for each orientation to achieve an equidistant phase difference for the 6-pixel period pattern. Therefore, 18 images are recorded in total for a SIM reconstruction. FairSIM [3] is used for three-beam interference SIM reconstruction. In contrast to a full 3D stack reconstruction, this software uses the OTF attenuation method to maintain the optical sectioning ability from only a single z-slice without compromising the lateral resolution improvement. This feature greatly simplifies the reconstruction process and increases the robustness of the reconstruction.

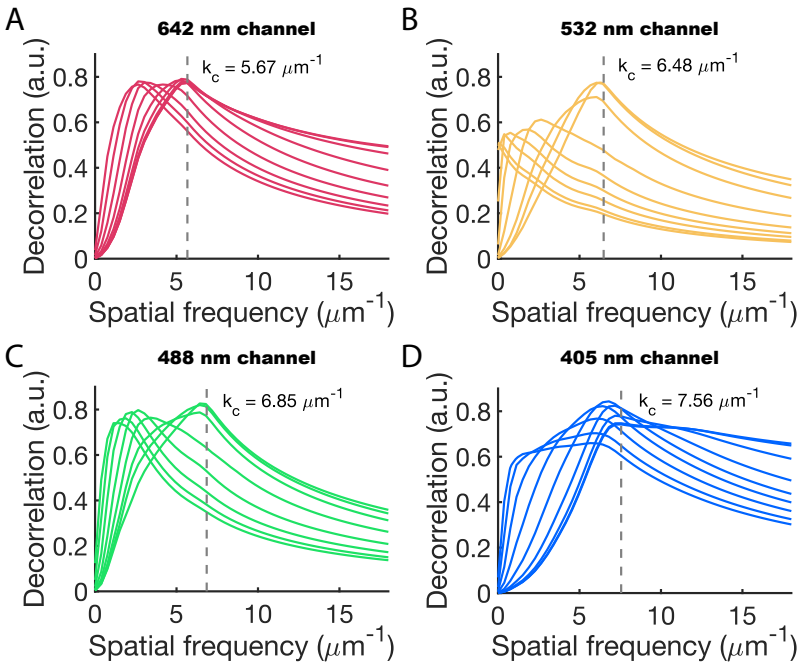


**Fig. S4.** Image decorrelation analysis [4] of the four channels of live cell imaging. 10 different cell images were analyzed. The resolution of each channel is determined to be: $176 \pm 7$ nm (642 nm channel); $154 \pm 3$ nm (532 nm channel); $146 \pm 4$ nm (488 nm channel); $134 \pm 6$ nm (405 nm channel). These results match well with the theoretical calculation and the FRC analysis presented and discussed in the main text.

## 7. LIVE CELL TIME SERIES IMAGING

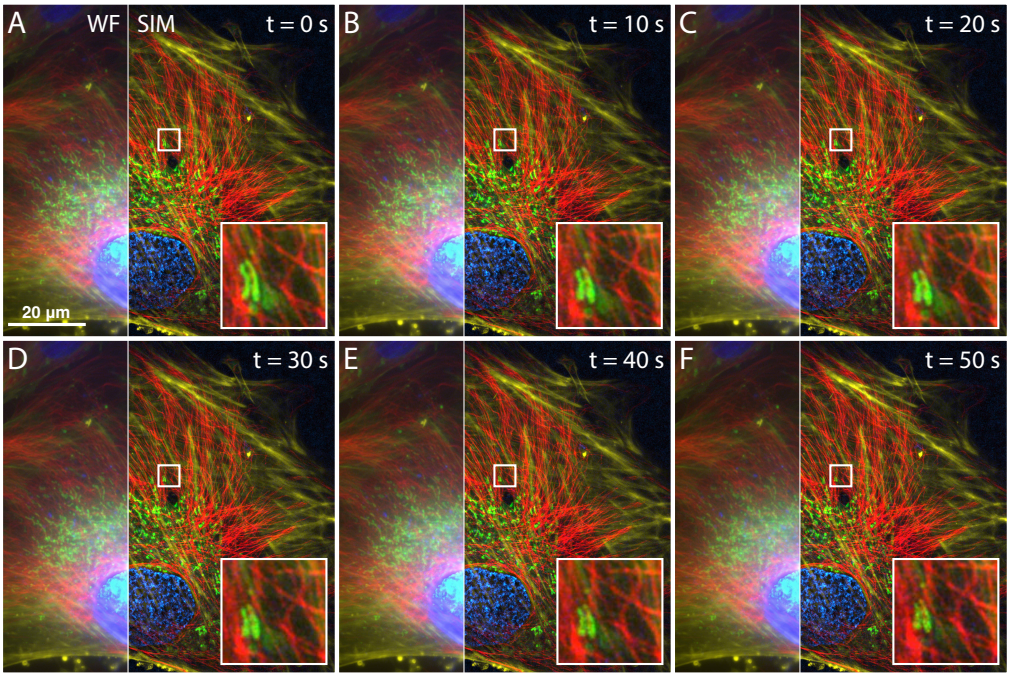


**Fig. S5.** Time series of 4-color SIM imaging of live human BJ fibroblast cells. Exposure time for each SIM raw image: 30 ms. The insets show the flunctuation of microtubule fibers and the morphology changes of mitochondria during the time window. For the four-color live cell imaging shown, the $4 \times 18 = 72$ subimages required for SIM reconstruction, at present, limits the SIM frame rate to 0.4 Hz. The 6 images are shown in 10 second intervals and with similar intensity and SNR indicating good capability for longer time imaging.

## REFERENCES


1. M. K. Giles, R. S. Hughes, and J. L. Thompson, "Angular Dispersion of Diffraction Gratings Used for Tuning Organic Dye Lasers," Appl. Opt. **12**, 421–422 (1973).
2. Y. Wu and H. Shroff, "Faster, sharper, and deeper: structured illumination microscopy for biological imaging," Nat. Methods **15**, 1011–1019 (2018).
3. M. Müller, V. Mönkemöller, S. Hennig, W. Hübner, and T. Huser, "Open-source image reconstruction of super-resolution structured illumination microscopy data in ImageJ," Nat. Commun. **7**, 10980 (2016).
4. A. Descloux, K. S. Grußmayer, and A. Radenovic, "Parameter-free image resolution estimation based on decorrelation analysis," Nat. Methods **16**, 918–924 (2019).